Nuclear and Magnetic Structures and Magnetic Properties of $Co_3(OH)_2(SO_4)_2(H_2O)_2$. Comparison to the Mn and Ni Analogues

Mohsen Ben Salah and Serge Vilminot*

Groupe des Matériaux Inorganiques, IPCMS, UMR CNRS-ULP 7504, 23 rue du Loess, BP 43, 67034 Strasbourg Cedex 02, France

Gilles André and Françoise Bourée-Vigneron

Laboratoire Léon Brillouin, CEA-CNRS, CEA Saclay, 91191 Gif-sur-Yvette Cedex, France

Mireille Richard-Plouet

Institut des Matériaux Jean Rouxel, 2 rue de la Houssinière, BP 32229, 44322 Nantes Cedex 03, France

Tahar Mhiri

Laboratoire de l'Etat Solide, Faculté des Sciences, 3038 Sfax, Tunisia

Mohamedally Kurmoo*

Laboratoire de Chimie de Coordination Organique, CNRS-UMR 7140, Tectonique Moléculaire du Solide, Université Louis Pasteur, 4 rue Blaise Pascal, 67000 Strasbourg Cedex 01, France

Received December 17, 2004. Revised Manuscript Received March 22, 2005

We report the synthesis, crystal structure derived from X-ray single crystal and neutron powder data at 300 K, infrared spectra, thermogravimetric analysis, and the magnetic properties of $Co_3(OH)_2(SO_4)_2(H_2O)_2$ and its deuterated (d_6-) analogue, as well as the magnetic structure from neutron powder data of the latter as a function of temperature. The structure consists of corrugated metal-hydroxide layers with intralayer μ^6-sulfate, and the layers are connected to one another by μ^4-sulfate. The magnetic properties exhibit a transition from a paramagnet to a canted-antiferromagnet at 42 K and display an unusual hysteretic spontaneous magnetization with temperature. The paramagnetic region is characterized by Curie constants of ∼9.5 emu K/mol and a Weiss constant of ∼ −70 K. From the remanant magnetization, extrapolated from the linear dependence of the isothermal magnetization with field, we estimate the canting angle to be <0.2°. Refinement of the magnetic structure from data collected on two different diffractomers (D20 at ILL, Grenoble, and G4.1 at CEA, Saclay) and considering the group analysis of Bertaut's, we find the moments to lie along the *c*-axis with complete compensation of the moments within one layer. The temperature dependence of the moments of the two cobalt atoms also reflects the hysteresis observed in magnetization. The magnetic model is in good agreement with magnetization measurements performed on an aligned single crystal along the three orthogonal axes of the orthorhombic unit cell.

Introduction

As part of our ongoing study of the chemistry and characterization by X-ray and neutron crystallography and magnetic properties of divalent transition metal hydroxy-sulfates, we have recently reported several phases of manganese, nickel, and copper.[1−4] These metals predominantly adopt octahedral geometry and therefore, the chemistry and crystallography are less complicated. Copper forms two phases,[1] antlerite $Cu_3(OH)_4SO_4$ and brochantite $Cu_4(OH)_6SO_4$, that are characterized by triple chains connected by sulfate for the former and layers made up of double chains connected by the sulfate for the latter; their magnetic properties are typically low dimensional in character with a 3D antiferromagnetic ordering with a small canting at low temperatures. Manganese forms several phases with $Mn_3(OH)_2(SO_4)_2(H_2O)_2$,[2] $Mn_2(OH)_2(SO_4)$,[3] and $Mn_5(OH)_8(SO_4)$ being the most abundant. They all display manganese-hydroxide network connected by the sulfates and are all canted-antiferromagnets. Nickel gives $Ni_3(OH)_2(SO_4)_2(H_2O)_2$[4] and

* Authors to whom correspondence should be addressed. S.V. e-mail: vilminot@ipcms.u-strasbg.fr. Tel: +33 3 88 10 71 28. Fax +33 3 88 10 72 47. M.K. e-mail: kurmoo@chimie.u-strasbg.fr.

(1) (a) Vilminot, S.; Richard-Plouet, M.; André, G.; Swierczynski, D.; Bourée-Vigneron, F.; Marino, E.; Guillot, M. *Cryst. Eng.* **2002**, *5*, 177−186. (b) Vilminot, S.; Richard-Plouet, M.; André, G.; Swierczynski, D.; Guillot, M.; Bourée-Vigneron, F.; Drillon, M. *J. Solid State Chem.* **2003**, *170*, 255−264. (c) Hawthorne, F. C.; Groat, L. A.; Eby, R. K. *Can. Mineral.* **1989**, *27*, 205−209. (d) Helliwell, M.; Smith, J. V. *Acta Crystallogr.* **1997**, *C53*, 1369−1371.

(2) Ben Salah, M.; Vilminot, S.; André, G.; Richard-Plouet, M.; Bourée-Vigneron, F.; Mhiri, T.; Kurmoo, M. *Chem. Eur. J.* **2004**, *10*, 2048−2057.

(3) Ben Salah, M.; Vilminot, S.; Mhiri, T.; Kurmoo, M. *Eur. J. Inorg. Chem.* **2004**, 2272−2276.

(4) Vilminot, S.; Richard-Plouet, M.; André, G.; Swierczynski, D.; Bourée-Vigneron, F.; Kurmoo, M. *Inorg. Chem.* **2003**, *42*, 6859−6867.

10.1021/cm047790m CCC: $30.25
Published on Web 04/23/2005

$Ni_5(OH)_6(SO_4)_2(H_2O)_4$ which contain nickel-hydroxide layers and are also canted-antiferromagnets. Cobalt shows more diversity in the range of compounds and complexity in structure; both related to the fact that tetrahedral and octahedral coordination geometries are energetically favorable for cobalt. Because the different phases of manganese, nickel, and copper have similar colors it is more difficult to separate them. In contrast, cobalt hydroxysulfates are more colorful but are numerous.[6] The crystals can be deep blue, purple, red, or pink depending on the molecular structures around the cobalt centers and the thickness of the crystals.[7,8] Furthermore, in the cobalt series, it is known that the alkaline cations, Na, K, Cs, and Rb, as well as NH_4, can be present in the structures.[9] There are at least five different phases and their characterizations are slowly coming into place. We have recently reported the structure and properties of a ferromagnetic phase, $Co_5(OH)_6(SO_4)_2(H_2O)_4$.[5] It consists of $Co_4(OH)_6$ brucite layers bridged by an inorganic $Co(H_2O)_4(SO_4)_2$ unit and is an easy plane magnet with a Curie temperature of 14 K. In this paper, we present the characterization of the second phase in this series with cobalt which is isostructural to $M_3(OH)_2(SO_4)_2(H_2O)_2$, M═Mn or Ni.

Feitknecht and colleagues[7] first reported two forms of cobalt hydroxysulfate: $CoSO_4 \cdot 3Co(OH)_2$ and $2CoSO_4 \cdot 3Co(OH)_2 \cdot 5H_2O$. The first being blue hexagonal leaflets with variable amount of water which when reacted with concentrated $CoSO_4$ resulted in violet crystals of the latter. Dubler and Oswald reexamined these reactions and reported another two phases, dark violet $Co_3(OH)_2(SO_4)_2 \cdot 2H_2O$ ($a = 7.207(2)$ Å, $b = 9.774(2)$ Å, $c = 12.861(3)$ Å, space group *Pbcm*)[8] and a series[9] with the general formula $M_2Co_3(OH)_2(SO_4)_3 \cdot 2H_2O$, with M being K^+, NH_4^+, Rb^+, Cs^+, or Tl^+. The corresponding Na^+ compound contains four H_2O molecules instead of two for the other cations.[10] These authors went on to fully characterize the former by single-crystal structure determination, infrared spectroscopy, and thermogravimetry, while Feitknecht and colleagues[7] reported the structural characterization of the salts containing alkali metal from powder diffraction. In a systematic study of the reaction of varying molar ratios of NaOH and $CoSO_4$ at different temperatures, Deweck[11] confirmed the existence of the blue phase as $CoSO_4 \cdot 3Co(OH)_2$ and a violet phase $2CoSO_4 \cdot 3Co(OH)_2 \cdot 3H_2O$ similar to the observations of Feitknecht and colleagues.[7] However, they point to the unreliable determination of the amount of water in the latter. Further studies were also carried out with mixed metals in the compound $M_4(OH)_6(SO_4)$, Zn, Co, and Ni.[12]

Using a different approach, Rosseinsky et al.[13] have prepared modifications of Namuwite,[14] $(Cu_{0.373}Zn_{0.627})_4(OH)_6(SO_4) \cdot 4H_2O$, with incorporated organic amines. They prepared two new phases containing Co−OH−SO_4 layers containing both tetrahedral and octahedral coordinated cobalt atoms bridged by ethylenediamine or dabco. Furthermore, these compounds were shown to be very stable and exhibit reversible dehydration and rehydration. They are canted antiferromagnets where the moments within one ferrimagnetic layer oppose those in the neighboring layers and show a further metamagnetic transition at fairly low applied fields. From analysis of the critical exponent of the metamagnetic critical field as a function of temperature, they were shown to be XY-easy plane magnets.

Our interest in the structures and magnetic properties of transition metal-hydroxysulfates stems from the fact that the hydroxide, in most cases, acts as μ^3 between the metal atoms providing very favorable M−O−M magnetic exchanges and the sulfate can coordinate as many as seven metal atoms but provide weaker exchanges through M−O−S−O−M. While the efficient exchange via the hydroxide has been found to give rise to layered magnets with Curie temperature up to 60 K,[15] the sulfate is more modest as found in the metal sulfates. In view of the different magnetic structures for the nickel[4] and manganese[2] compounds belonging to the $M_3(OH)_2(SO_4)_2(H_2O)_2$ family, which may be associated with the different single ion anisotropy, the present study on the cobalt analogue was undertaken to complete the set, especially with a cation having a higher magnetic anisotropy. We should point out that the magnetic structure of the nickel compound is temperature independent while that of the manganese is not. In addition, the latter shows the unusual coexistence of both long range and short range orderings in the same temperature regime.

Experimental Section

Sample Preparation. Analar-grade chemicals were used for all syntheses. $Co_3(OH)_2(SO_4)_2(H_2O)_2$ was prepared by hydrothermal treatment of an aqueous suspension (20 mL) obtained by mixing solutions of cobalt(II) sulfate hepta-hydrate $CoSO_4 \cdot 7H_2O$ (2.5 g, 8.9 mmol) and sodium hydroxide (0.178 g, 4.5 mmol), that is in a Co/Na molar ratio (2:1), at 245 °C for 10 h under autogenous pressure in 125-mL Teflon-lined autoclaves. After the autoclave was quench cooled in water, the solid products were separated from their mother liquor and washed several times with water, alcohol, and acetone before drying in air. The title compound was obtained as transparent purple rectangular plates with, in some cases, a small amount of blue crystals that were easily separated. There are several other byproducts that are worth mentioning. Due to the formation

(5) Ben Salah, M.; Vilminot, S.; Richard-Plouet, M.; André, G.; Mhiri, T.; Kurmoo, M. *Chem. Commun.* **2004**, 2548−2549.
(6) Ben Salah, M. Ph.D. Thesis, Université Louis Pasteur, Strasbourg, France, 2004.
(7) Feitknecht, W. *Helv. Chim. Acta* **1933**, *16*, 427−54. Feitknecht, W.; Fischer, G. *Helv. Chim. Acta* **1935**, *18*, 40−60.
(8) Dubler, E.; Oswald, H. R. *Naturwissenschaften* **1969**, *56*, 327.
(9) Dubler, E.; Oswald, H. R. *J. Appl. Crystallogr.* **1970**, *3* (3), 175−178.
(10) (a) Dubler, E.; Oswald, H. R. *Helv. Chim. Acta* **1971**, *54* (6), 1621−1628. (b) Dubler, E.; Oswald, H. R. *Helv. Chim. Acta* **1971**, *54* (6), 1628−1637.
(11) Deweck, J. *Metallurgie* **1969**, *9* (2), 49−57.
(12) (a) Lecocq, R.; Glibert, J.; Breckpot, R. *Bull. Soc. Chim. Belges* **1971**, *80* (9−10), 563−584. (b) Frias Ferreira da Rocha, M.; Glibert, J. *Bull. Soc. Chim. Belges* **1973**, *82* (1−2), 63−73. (c) Frias Ferreira da Rocha, M.; Glibert, J. *Bull. Soc. Chim. Belges* **1973**, *82* (3−4), 165−177. (d) Martinez, M. A.; Ramirez Garcia, A.; Garcia Martinez, O. *Anal. Quim.* **1975**, *71* (6), 574−581.
(13) (a) Rujiwatra, A.; Kepert, C. J.; Claridge, J. B.; Rosseinsky, M. J.; Kumagai, H.; Kurmoo, M. *J. Am. Chem. Soc.* **2001**, *123*, 10584−10594. (b) Rujiwatra, A.; Kepert, C. J.; Rosseinsky, M. J. *Chem. Commun.* **1999**, 2307.
(14) (a) Groat, L. A. *Am. Mineral.* **1996**, *81*, 238−243. (b) Bevins, R. E.; Turgoose, S.; Williams, P. A. *Mineral. Mag.* **1982**, *46* (338), 51. (c) Bear, I. J.; Grey, I. E.; Madsen, I. C.; Newnham, I. E.; Rogers, L. J. *Acta Crystallogr., Sect. B* **1986**, *42*, 32.
(15) Kurmoo, M.; Kumagai, H.; Hughes, S. M.; Kepert, C. J. *Inorg. Chem.* **2003**, *42*, 6709.

of a green layered hydroxide carbonate of Co^{2+} in alkaline solution which decomposes to brown Co_3O_4 at high temperatures, freshly boiled distilled water free of soluble carbon dioxide was used and the reactor was immediately sealed after mixing the cobalt sulfate and sodium hydroxide solutions. These precautions do not always preclude the formation of cobalt oxides, therefore, the samples were examined under an optical microscope and crystals contaminated with cobalt oxides were then discarded. When mixing the cobalt sulfate and sodium hydroxide solutions a voluminous blue suspension is always formed in a pink solution. Diffraction patterns of both the blue suspension and the blue crystals mentioned above appear similar; consisting of only one broad diffraction peak at around $d = 9.59$ Å in the former developing into a series of harmonics based on the line at 9.59 Å for the latter, suggesting a layered structure. Infrared and TGA of both samples reveal that they contain OH and SO_4 groups. The purple plate crystals of $Co_3(OH)_2(SO_4)_2(H_2O)_2$ turn blue-green when suspended in water for a few days and the solution turns pink. The diffraction pattern of these crystals also displays only one broad peak at 9.6 Å as that of the blue suspension. Most importantly, a ferromagnetic phase, $Co_5(OH)_6(SO_4)_2(H_2O)_4$, is also obtained depending on the temperature of the reaction and the concentration of reagents.[5] It is formed as irregular thin pink plates. However, this phase is quite difficult to remove and most samples were found to have about ca. 0.1%. Another paramagnetic pink hexagonal plate phase is also formed at higher pH and can be easily avoided in the preparation and removed when present.

Samples for neutron powder diffraction were prepared using the above conditions and replacing water (H_2O) by heavy water (D_2O). The substitution of H by D is to reduce the high incoherent scattering by hydrogen giving rise to an increase of the background that can perturb further analysis. IR spectra and final refinement of high quality neutron diffraction data at 300 K reveal that D for H substitution has been achieved with a good yield.

Physical Techniques. Differential thermal (DT) and thermogravimetric (TGA) analyses were performed in air on a TA-SDT-Q600 apparatus, at a heating rate of 5 °C/minute. Infrared spectra were recorded by use of an ATI Mattson spectrometer by transmission through a KBr pellet containing ca. 1% of the compound. The spectra were recorded at a resolution of 4 cm^{-1} in the range 500−4000 cm^{-1}. The UV−visible spectrum was recorded on a Hitachi U-3000 spectrometer by transmission through an array of crystals held in a PMMA matrix. Powder X-ray diffraction patterns were recorded using a D500 Siemens diffractometer (Co $K\alpha_1$ radiation, $\lambda = 1.789$ Å). Temperature dependence diffraction data were obtained by use of an INEL multichannel diffractometer (Co $K\alpha_1$ radiation, $\lambda = 1.789$ Å).

X-ray Crystallography and Nuclear Structure Refinement. Single-crystal X-ray data were collected at room temperature on a selected crystal mounted on a glass fiber. A single set of 180 frames (each frame measured twice), 20 s/frame, phi scan of 1 deg/frame, crystal detector distance = 30 mm, theta = 0 deg, kappa = 0 deg was collected on a Nonius Kappa CCD diffractometer at the Service Commun de Rayons X, Université Louis Pasteur, Strasbourg. Structure refinement has been performed starting from the atomic positions of the corresponding nickel compound[4] using SHELXL-93.[16] The final refinement includes anisotropic displacement parameters and the empirical extinction correction within SHELXL-93 that include abnormal absorption and mosaicity extinction. The atomic coordinates of the hydrogen atoms were found from the difference Fourier maps and were refined with isotropic displacement parameters. Additional experimental details are given in Table 1 and in the Supporting Information (SI). Table S1 (in the SI) lists the fractional atomic coordinates and Table 2 gives the bond distances and angles from X-ray refinement. For convenience, the oxygen atoms of the sulfate group, of the hydroxyl groups, and of the water molecule are labeled O, OH, and OW, respectively. For H [D for neutron data] atoms, H(1)[D(1)] and H(2)[D(2)] correspond to OH(1)[OD(1)] and OH(2)[OD(2)] groups, respectively, whereas HW [DW] refers to the H[D] atoms of the water molecule. The structural data have been deposited at the Fachinformationszentrum (FIZ) Karlsruhe and have been given CSD number 41-4487.

Table 1. Summary of X-ray Data Collection on a Single Crystal and Structure Refinement of $Co_3(OH)_2(SO_4)_2(H_2O)_2$

a (Å)	7.1959(2)	μ (mm^{-1})	6.01
b (Å)	9.7542(3)	total reflns	2892
c (Å)	12.8326(4)	unique reflns	1501
V ($Å^3$)	900.72(8)	unique $\lvert F_o\rvert > 4\sigma(F_o)$	1297
Z	4	R_{int}	0.0274
space group	*Pbcm* (No. 57)	R(F) (all data)[a]	0.0375
F (000)	876	w$R(F_o^2)$ (all data)[b]	0.0737
D_c ($g\cdot cm^{-3}$)	3.235	GOF	1.10

[a] $R(F) = \sum\lvert\lvert F_o\rvert - \lvert F_c\rvert\rvert/\sum\lvert F_o\rvert$. [b] $wR = \{\sum[w(F_o^2 - F_c^2)^2]/\sum[w(F_o^2)^2]\}^{1/2}$, $w = 1/[\sigma^2(F_o^2) + (0.0262P)^2 + 1.2P]$ with $P = (\mathrm{Max}(F_o^2,0) + 2F_c^2)/3$.

The neutron diffraction experiments were performed at the Laboratoire Léon Brillouin (CEA, Saclay) using the G4.1 and 3T2 diffractometers. The multi-detector (800 cells) G4.1 powder diffractometer ($\lambda = 2.4266$ Å) was used for the determination of the magnetic structure and the study of the temperature dependence of the magnetic structure in the ordered state. A total of 14 diffraction patterns were recorded in the 2θ range 10−89.9°, at different fixed temperatures between 1.4 and 70 K. The powder sample was held in a cylindrical vanadium container placed in a helium cryostat. The room-temperature structure refinement was performed from data collected on the same sample using the high-resolution 3T2 diffractometer ($\lambda = 1.2522$ Å). Additional data on cooling and warming in the temperature range 50 to 2 K have been recorded on a second sample on the D20 diffractometer ($\lambda = 2.419$ Å) at the Laue Langevin Institut (Grenoble). Nuclear and magnetic structures were refined using the FULLPROF suite of programs.[17] The nuclear scattering lengths ($b_{Co} = 0.2490 \times 10^{-12}$ cm, $b_S = 0.2847 \times 10^{-12}$ cm, $b_O = 0.5803 \times 10^{-12}$ cm, $b_D = 0.6671 \times 10^{-12}$ cm, and $b_H = -0.3739 \times 10^{-12}$ cm) and cobalt magnetic form factors were those included in the program.

Magnetization Measurements. Magnetization measurements were performed on several samples of both the hydrogenated and deuterated compounds. Because of the presence of several transitions arising from multiphase samples, the magnetic susceptibility measurements were finally performed on crystals of well-defined morphology, which were selected under an optical microscope and washed carefully with ethanol. Data were taken on cooling by means of a Quantum Design MPMS-XL SQUID magnetometer. Isothermal magnetization was measured at 2 K in field spanning ±50 kOe. AC magnetization measurements were performed using the same apparatus in zero dc field and an alternating field of 1 Oe oscillating at 17 Hz.

Results and Discussion

Synthesis. As already pointed out in the literature[7−10] the chemistry of cobalt-hydroxysulfate is quite rich compared to that of other metals and this richness provides not only

(16) Sheldrick, G. M. SHELXL-93, Program for the Refinement of Crystal Structures, University of Göttingen, Germany, 1993.

(17) Rodriguez-Carvajal, J. FULLPROF: Rietveld, profile matching and integrated intensity refinement of X-ray and/or neutron data, 3.5d version. Léon-Brillouin Laboratory, CEA Saclay, France, 1998.

Table 2. Interatomic Distances (Å) and Angles (deg) from X-ray Structure Determination (upper part) and Involving D Atoms from Neutron Powder Diffraction Data at 300 K (lower part)

From X-ray Structure Determination					
S1−O3	1.459(2) × 2	O3−S1−O3	107.46(15)	O2−S1−O2	108.42(15)
S1−O2	1.494(2) × 2	O3−S1−O2	110.19(10) × 2	⟨O−S1−O⟩	109.5
⟨S−O⟩	1.477	O3−S1−O2	110.29(10) × 2		
S2−O4	1.461(2)	O4−S2−O1	110.83(15)	⟨O−S2−O⟩	109.5
S2−O1	1.478(3)	O4−S2−O5	108.45(9) × 2		
S2−O5	1.482(3) × 2	O1−S2−O5	110.01(10) × 2		
⟨S−O⟩	1.476	O5−S2−O5	109.05(16)		
Co1−O5	2.067(2)	O5−Co1−OH1	94.58(9)	OH1−Co1−O2	102.34(7)
Co1−OH1	2.068(2)	O5−Co1−OW	166.20(8)	OW−Co1−OH2	104.94(10)
Co1−OW	2.068(2)	O5−Co1−OH2	88.10(9)	OW−Co1−O2	84.35(8)
Co1−OH2	2.108(2)	O5−Co1−O2	88.90(7)	OW−Co1−O2	85.04(8)
Co1−O2	2.179(2)	O5−Co1−O2	81.75(7)	OH2−Co1−O2	100.45(7)
Co1−O2	2.210(2)	OH1−Co1−OW	92.09(10)	OH2−Co1−O2	169.64(7)
⟨Co1−O⟩	2.087	OH1−Co1−OH2	80.40(8)	O2−Co1−O2	77.44(7)
		OH1−Co1−O2	176.45(9)		
Co2−O3	2.047(2) × 2	O3−Co2−O3	166.47(11)	OH1−Co2−O4	94.87(10)
Co2−OH1	2.063(3)	O3−Co2−OH1	90.99(5) × 2	OH1−Co2−O1	173.28(10)
Co2−OH2	2.072(3)	O3−Co2−OH2	96.63(5) × 2	OH2−Co2−O4	172.20(11)
Co2−O4	2.123(2)	O3−Co2−O4	83.25(5) × 2	OH2−Co2−O1	93.79(11)
Co2−O1	2.148(2)	O3−Co2−O1	88.23(5) × 2	O4−Co2−O1	78.41(10)
⟨Co2−O⟩	2.083	OH1−Co2−OH2	92.93(11)		
Co1···Co1	3.124(2)	Co1−OH1−Co1	98.1(1)	Co1−O2−Co1	102.6(1)
Co1···Co1	3.424(2)	Co1−OH2−Co1	95.6(1)	Co1−OH1−Co2	123.9(2)
				Co1−OH2−Co2	118.9(2)
From Neutron Powder Diffraction Data					
OD1−D1	0.94(1)	D1···O1	1.98(1)	OD1−D1···O1	175(3)
OD2−D2	0.97(1)	D2···O5	2.35(1) × 2	OD2−D2···O5	145(3) × 2
OW−DW1	0.95(1)	DW1···O3	2.18(1)	OW−DW1···O3	150(3)
		DW1···O4	2.434(9)	OW−DW1···O4	127(1)
OW−DW2	0.930(9)	DW2···O5	2.15(1)	OW−DW2···O5	147(2)
DW1−DW2	1.53(1)	DW1−OW−DW2	109(2)		

many compounds for study but also difficulties in characterization, especially when the measurements require large quantities of single-phase materials. It is also important to note that certain phases are prepared starting from another one in the presence of concentrated cobalt sulfate or by suspension in water. However, by careful choice of concentration of reactants, temperature, and time of the hydrothermal reactions, we were only able to isolate single phases with some difficulty. This was possible after carefully mapping the three parameters.

Powder X-ray Diffraction. The X-ray powder diffraction pattern is similar to that of the corresponding nickel and manganese samples, having the same sequence of diffraction peaks, whose *d*-spacing falls between the corresponding values for Ni and Mn samples. This observation is in agreement with the corresponding ionic radii, Ni^{2+} 0.74 Å, Co^{2+} 0.80 Å, Mn^{2+} 0.95 Å, resulting in a variation of the unit cell parameters according to the corresponding M−O bond distances. The diffraction pattern and the refined unit cell parameters also agree with the results reported by Dubler and Oswald.[8]

Powder X-ray Diffraction at Variable Temperature. From 25 to 170 °C, the X-ray diffraction pattern corresponds to that of $Co_3(OH)_2(SO_4)_2(H_2O)_2$. At 220 °C (Figure S1 in the SI), an additional phase is formed corresponding to $Co_3(OH)_2(SO_4)_2$ according to the TGA data. The transformation to this dehydrated form is complete at 270 °C and the crystals are stable up to 400 °C. Between 460 and 520 °C, a mixture of CoO and β-$CoSO_4$ is evidenced. Finally, CoO is the principal product observed between 600 and 700 °C, the high-temperature limit. These results confirm the thermal evolution observed in TGA; the differences in temperature being related to different heating procedures. However, Co_3O_4 is not observed in this experiment in contrast to the results from TGA. This is due to the absence of oxygen in the reduced-pressure atmosphere in the X-ray experiment, whereas for TGA the flow of air results in the oxidation of CoO. Attempts to index the pattern of the anhydrous $Co_3(OH)_2(SO_4)_2$ phase were not successful.

Thermal Analysis. The TGA trace recorded in air at a heating rate of 5 °C/min shows four successive weight losses (Figure S2). The first, centered at 350 °C, and the second at 500 °C are attributed to departure of the coordinated water and of OH groups as H_2O, respectively. However, the corresponding weight losses are not in the expected 2:1 ratio, but a value close to 3:1 is observed. This has been explained by the oxidation of CoO, obtained after hydroxyl group removal, into Co_3O_4 and results in a weight gain. This result has been confirmed by XRD on a sample previously annealed at 600 °C for 20 min using the same heating rate. In addition to Co_3O_4, the XRD reveals the presence of β-$CoSO_4$. The first weight loss, related to the departure of water molecules, starts at around 240 °C and progresses into the large step starting at 330 °C. A similar observation was made by Dubler and Oswald[10] who have related it to the granulometry of the sample. We performed DT-TGA analysis on a few single crystals and observed the disappearance of the progressive weight loss below 330 °C. On the other hand, Dubler and Oswald[10] proposed the formation of $Co_3O(SO_4)_2$ after the second weight loss. On account of X-ray diffraction data at variable temperatures, the presence of this compound cannot be confirmed. Furthermore, the diffraction pattern corresponds to a superposition of those of CoO and β-$CoSO_4$. The third weight loss at 840 °C is associated with $CoSO_4$

decomposition. Again, the observed loss is smaller than that expected in relation with the oxidation of CoO into Co_3O_4. Finally, the fourth weight loss corresponds to the reduction of Co_3O_4 into CoO. From the residual mass, the estimated cobalt weight content of the compound is 40.2% for a theoretical value of 40.3%.

Infrared and UV−Visible Spectroscopies. The IR spectra recorded on the H and D samples are presented on figure S3 (SI). The comparison of two spectra allows one to distinguish between vibration bands related to OH and H_2O groups that are shifted in the D sample with a factor of $(18/17 \times 2)^{1/2}$ and vibration bands of the SO_4 groups that do not.

In the O−H valence vibration region, three bands at 3549, 3479, and 3438 cm^{-1} and a shoulder at 3576 cm^{-1}, are observed, but only two, at 2640 and 2542 cm^{-1}, are observed for the corresponding O−D vibrations. Water is clearly evidenced by the presence of the bending mode as a sharp band at 1620 cm^{-1}. Although the shoulder at 1597 cm^{-1} may suggest the presence of an impurity, the IR spectra recorded on selected crystals do not reveal any change in the respective intensities. Two other bands at 852 and 813 cm^{-1}, which disappear in the D compound, have been related to rocking vibration modes of the water molecules.[18]

For the sulfate groups, three bands appear in the regions related to ν_3 (1186, 1160, and 1108 cm^{-1}) and ν_4 (642, 625, and 597 cm^{-1}) vibrations. As the symmetry of the SO_4 is lowered from the regular T_d symmetry, either on coordination (to C_{3v} for unidentate and C_{2v} for bidentate or bridging) or by distortion, the ν_1 (A_1) which is only Raman active first becomes IR and Raman active and the ν_3 (T_2) band splits into three IR and Raman active components (A_1, B_1, and B_2). The last two bands at 1029 and 991 cm^1 have been attributed to ν_1 mode that becomes IR active when the symmetry is lowered. Our results agree very well with those of Dubler and Oswald.[10]

The UV−visible spectrum (Figure S4) of $Co_3(OH)_2(SO_4)_2(H_2O)_2$ was recorded by transmission through an array of crystals held in a PMMA matrix. The spectrum is characterized by two absorption bands at 486 and 536 nm: the first originating from the $^4T_{1g}(F) \rightarrow {}^4T_{1g}(P)$ and the second from the $^4T_{1g}(F) \rightarrow {}^4A_{2g}$ transition. The two transitions appear to be considerably more intense compared to compounds with regular octahedral geometry or Co(II) in solution.

Single-Crystal X-ray Structure and Rietveld Refinement of Neutron Diffraction Powder Data at 300 K. The structure of $Co_3(OH)_2(SO_4)_2(H_2O)_2$ is globally the same as that of the corresponding nickel and manganese compounds.[2,4] It is also in good agreement with those reported by Dubler and Oswald.[10] In addition, we precisely located the hydrogen atoms, especially from the neutron powder data. The key feature of this structure is the corrugated sheets of octahedrally coordinated cobalt connected by the sulfate groups. The sheets, parallel to the *bc*-plane (Figure 1), consist of edge-sharing zigzag chains of Co(1) along *c*-axis connected by the apexes of Co(2). Also within the layer are the OH-groups acting as μ^3-connectors between two Co1 and one Co2 and one of the sulfate group (S1) acting as μ^6 bridging four Co1 and two Co2, while the water molecules are terminal on Co1. The second sulfate (S2) is μ^4 and bridges adjacent layers via two Co1 and one Co2 of one to a Co2 on the other. This results in a highly dense 3D-structure (Figure 2). The octahedra around Co(1) atoms, i.e., within the chains and consisting of three sulfate groups, two hydroxide, and one water oxygen atoms, are more distorted than that of Co2 which consists of four sulfate and two hydroxide oxygen atoms. We should note that the hydroxides

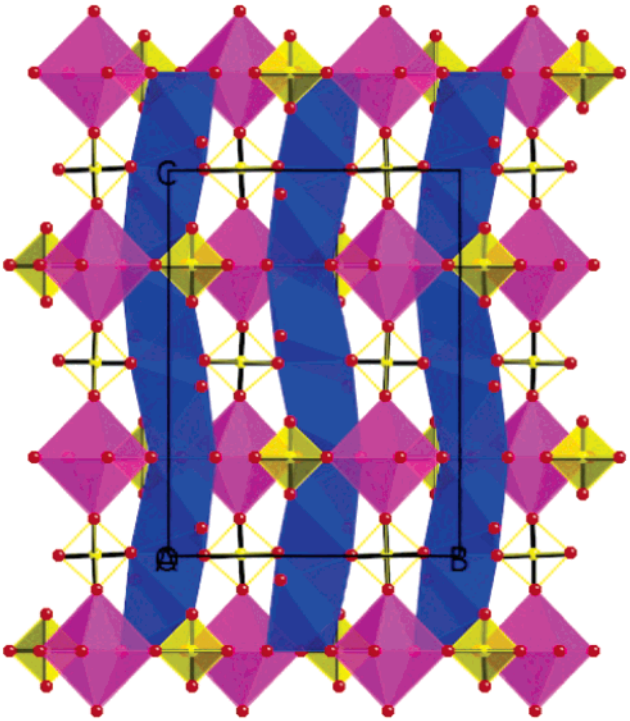

Figure 1. Structure of $Co_3(OH)_2(SO_4)_2(H_2O)_2$: polyhedral view of the layers along the *a*-axis (Co1, blue; Co2, purple; sulfate 1, open; sulfate 2, filled).

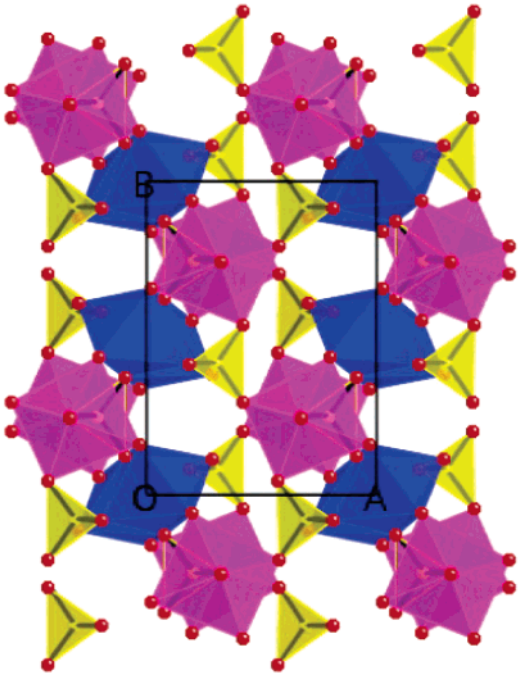

Figure 2. View of the structure of $Co_3(OH)_2(SO_4)_2(H_2O)_2$ along the *c*-axis.

(18) Nakagawa, I.; Shimanouchi, T. *Spectrochim. Acta* **1964**, *20*, 429.

Table 3. Summary of the Crystallographic Data and Refinement Characteristics at 300 and 1.4 K from Neutron Powder Data for the Deuterated Compound

	300	1.4
system	orthorhombic	
space group	*Pbcm* (57)	
a (Å)	7.2007(3)	7.2214(4)
b (Å)	9.7626(4)	9.7395(4)
c (Å)	12.8421(4)	12.8287(6)
wavelength (Å)	1.2252	2.4266
2θ range and step	6−125.7° 0.05°	10−89.9° 0.1°
reflns	1614	574
no. of params	75	53
R_p (%)	13.1	11.5
R_{wp} (%)	13.7	12.3
R_{exp} (%)	6.45	1.83
R_B (%)	8.15	5.20
R_F (%)	4.36	3.34
GOF (%)	4.52	
$R_{magnetic}$ (%)		7.58

are always in *cis*-configuration. The sulfate tetrahedra are nearly regular (Table 2). The refinement from neutron powder data recorded at 300 K allows one to obtain precise positions of the deuterium atoms as well as the respective H and D proportions (Tables 3 and S2, figure S5). All O−D bond lengths are close to a mean value of 0.95 Å and the D atoms are involved in weak deuterium bonds, with the shortest D···O distance being 1.98 Å between D1 and O1.

Magnetic Properties. The magnetic properties of $Co_3(OH)_2(SO_4)_2(H_2O)_2$ were, in the early stage of this study, hampered by the observation of multiple long-range magnetic transitions due to the presence of several crystallographic phases. Consequently, we were forced, as in the case of the nickel and manganese analogues, to select single crystals of each phase in order to complete the information on their magnetic properties as a function of temperature and of applied magnetic field. However, to obtain absolute values of Curie constant and saturation magnetization we had to use a selection of several crystals with a measurable mass and so we could not avoid the presence of trace amount of other phases. The results will be presented first for polycrystalline samples, and second for the single crystals.

The magnetic susceptibilities of polycrystalline samples of the hydrogenated (3.97 mg) and deuterated (26.72 mg) compounds were measured in an applied field of 100 Oe on cooling from 300 to 2 K. The results are shown in Figure 3. The data above 150 K were analyzed by the Curie−Weiss function which gave Curie constants of 9.19(5) emu K/mol for the H-compound and 9.70(2) emu K/mol for the D-compound and Weiss constants of −68(2) and −79(1) K, respectively. These Curie constants are within the range observed for divalent cobalt in octahedral coordination geometry. Both compounds exhibit a strong and sharp peak in the susceptibility at 42 K followed by another anomalous rise centered at 15 K. The peak at 42 K was found to be intrinsic to the $Co_3(OH)_2(SO_4)_2(H_2O)_2$ and $Co_3(OD)_2(SO_4)_2(D_2O)_2$ compounds (see discussion on single crystal measurements later), while the anomaly at 15 K is due to the long-range ordering of the ferromagnetic phase, $Co_5(OH)_6(SO_4)_2(H_2O)_4$.[6] The dramatic change in magnetization at 42 K is accompanied by both real and imaginary components of the ac-susceptibility measured in a 1 Oe field oscillating at 17 Hz (Figure 4). These are very sharp indeed (<0.5 K).

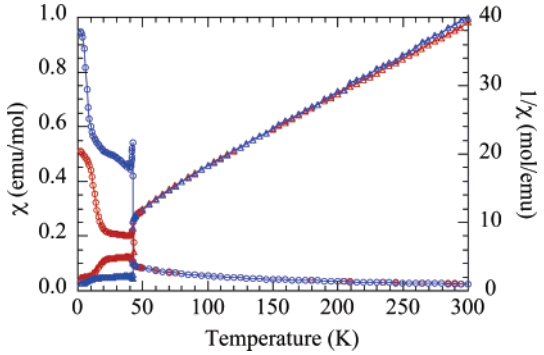

Figure 3. Temperature dependence of the magnetic susceptibility (circles) and its inverse (triangles) for polycrystalline samples of $Co_3(OH)_2(SO_4)_2(H_2O)_2$ (red) and $Co_3(OD)_2(SO_4)_2(D_2O)_2$ (blue).

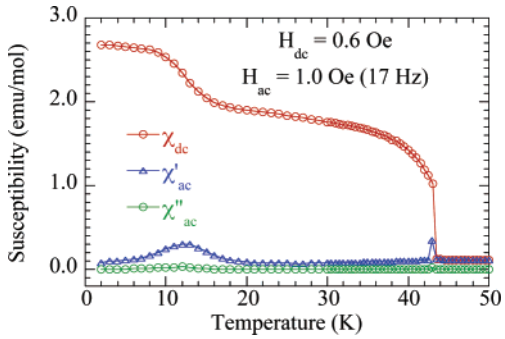

Figure 4. Temperature dependence of the dc- and ac-magnetizations in applied field of ca. 1 Oe for a polycrystalline sample of $Co_3(OD)_2(SO_4)_2(D_2O)_2$.

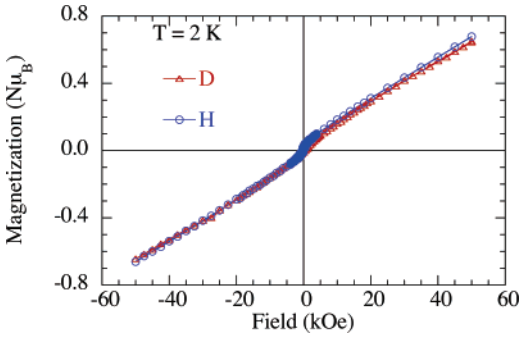

Figure 5. Isothermal magnetization at 2 K for polycrystalline samples of $Co_3(OH)_2(SO_4)_2(H_2O)_2$ and $Co_3(OD)_2(SO_4)_2(D_2O)_2$.

Figure 4 also presents the data of dc-susceptibility upon cooling in a field of 1 Oe, clearly showing the two transitions. The isothermal magnetizations of the two compounds (Figure 5) show linear dependence with field, attaining values approaching 0.7 μ_B at 50 kOe. Also apparent is a small hysteresis with a coercive field of ca. 350 Oe and remanant magnetization of 0.025 μ_B. All these magnetic properties, negative Weiss constant, linear dependence of isothermal magnetization in the ordered state, no saturation limit, and sharp anomaly in the ac-susceptibilities, are characteristics of a canted-antiferromagnet (also presented as "weak ferromagnet" in the literature). From the remanant field we can estimate, assuming a two-sublattice antiferromagnet and a value of 9 μ_B if all the moments were aligned parallel, a canting angle of 0.2°. We should point out that the amounts of the ferromagnetic phase present in the two samples are less than 0.1% as judged from the saturation and remanant magnetizations of the latter.

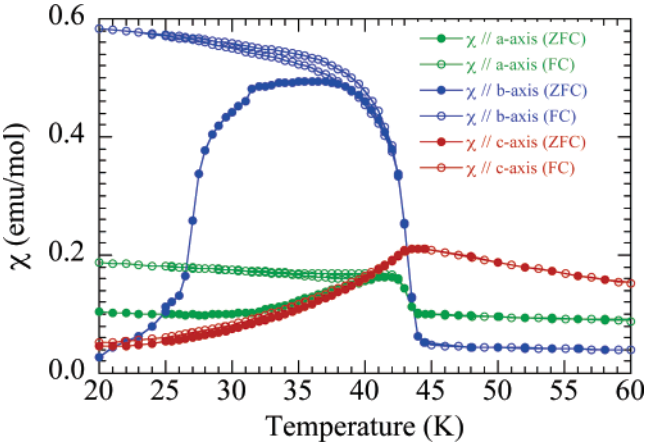

Figure 6. Temperature dependence of the susceptibility of single crystal 1 of $Co_3(OH)_2(SO_4)_2(H_2O)_2$ along its three orthogonal axes of the orthorhombic cell. The data were taken on warming and cooling in 1 kOe after zero field cooling the sample.

Measurements were performed on three independent single crystals selected under the microscope. Each crystal was first cast in poly(methyl methacrylate) (PMMA) from dichloromethane in a flat-bottom plastic beaker. The polymer with a crystal in the middle was then cut into a square bit of 4 × 4 mm^2. These were then aligned in the plastic straw with the applied field parallel to the different crystallographic axis. The axes were determined from Laue photographs allowing one to index the crystal faces and to orient them with respect to the magnetic field. The data taken on the three crystals were similar apart from slight misalignment and the presence of a small fragment of the ferromagnetic phase being present in crystal 1. The data taken on crystal 1, in a field of 1 kOe and in zero-field/field cooling procedures, along the three orthogonal crystallographic axes are shown in Figure 6. We note that the transition at 42 K is clearly observed. First, we see that the spontaneous magnetization is stronger along the *b*-axis, intermediate along the *a*-axis, and not present along the *c*-axis. From this we can infer that the easy axis lies along the crystallographic *c*-axis, the canting is along the *b*-axis, and the intermediate axis is along the *a*-axis. Please note that the ZFC−FC is reversible above 42 K and nonreversible below. Another unusual observation to be made is the hysteresis that is observed in field-cooling and field-warming runs starting at T_N down to 20 K. More details concerning this effect will be given below. There appears to be noticeable anisotropy even in the high-temperature paramagnetic regime. Analysis of the data above 150 K (Figure S6) gives C = 12.7(1) emu K/mol, $\theta = -77(3)$ K along the *a*-axis, C = 4.73(7) emu K/mol, $\theta = -39(4)$ K along the *c*-axis, and C = 8.4(1) emu K/mol, $\theta = +19(3)$ K along the *b*-axis. It is therefore clear that the anisotropy exists even to high temperatures. We also note that the Weiss constants vary from positive (ferromagnetic exchange) to negative (antiferromagnetic exchange). The presence of such differing magnetic properties may be the source of the canting in the ground state.

Crystal 2 exhibits similar behavior above 20 K and without any anomaly below due to the absence of the ferromagnetic phase. Unfortunately, only part of the data were collected because the crystal broke during the experiment.

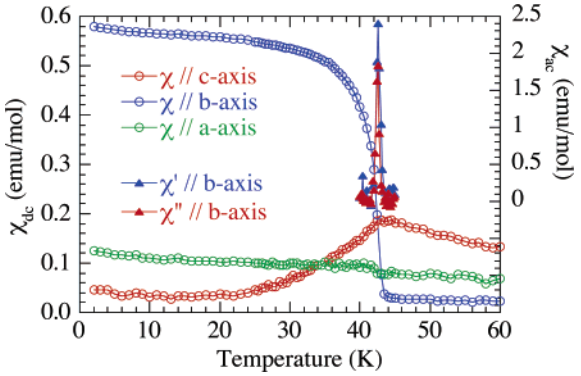

Figure 7. Anisotropy in the temperature dependence of the susceptibility of single crystal 3 of $Co_3(OH)_2(SO_4)_2(H_2O)_2$ measured on cooling in 1 kOe dc-field along its three orthogonal axes of the orthorhombic cell. Ac-susceptibilities (1 Oe, 17 Hz) are shown only around the transition at 43 K for H//*b*-axis; there is no anomaly for H//*a* or *c*.

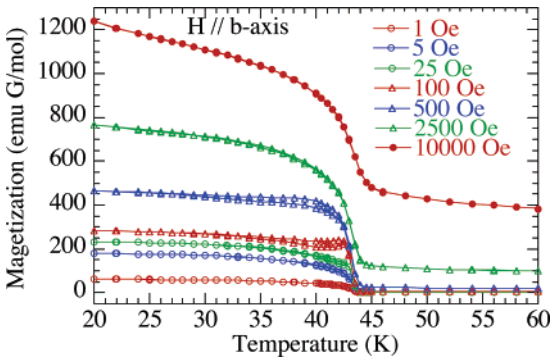

Figure 8. Field dependence of the hysteresis observed in the magnetization of single crystal 1 of $Co_3(OH)_2(SO_4)_2(H_2O)_2$ along the *b*-axis.

The data taken in a field of 1 kOe along the three crystallographic axes of crystal 3 are shown in Figure 7. Figure 7 also shows the ac-susceptibilities with the field applied parallel to the *b*-axis in the vicinity of the transition at 42 K. We note the similarity of the results with those of crystal 1 and also the more accurate alignment along the *a*-axis as well as the absence of the second transition below 15 K originating from the ferromagnetic phase $Co_5(OH)_6(SO_4)_2(H_2O)_4$. As pointed out earlier, we observed a hysteresis in the temperature dependence of the magnetization upon field-cooling and subsequent warming in the same field. The hysteresis is present in all three directions, though to different degrees. We therefore studied the effect of the applied field on this anomaly. This is shown in Figure 8. We first note the shape of the anomaly as a function of field. It appears normal in very low fields and there is very little hysteresis. On increasing the field to 100 Oe, there appears a peak and the hysteresis becomes more prominent. On increasing the field further the curves revert back to be rounded without hysteresis. We also observe minor loops within the major loop (Figure S7). In our view, such behavior has not been previously reported for any magnet. This suggests that there is a first-order transition associated with the Néel ordering of the moments.

Magnetic Structure Determination. The magnetic structure was solved from neutron powder diffraction data collected at 1.4 K. Its thermal evolution has been followed from data collected at 14 temperatures ranging between 1.4 and 70 K. The comparison of the data collected at 1.4 K

Table 4.

atom	M//*a*	M//*b*	M//*c*
Co11 − Co18	+ − + − + − + −	+ − + − − + − +	+ − − + − + + −
Co21 − Co24	0	0	+ − + −

with the corresponding ones for Mn reveals a great analogy. Therefore, the same structural model for the magnetic structure has been used. The corresponding model obtained by applying Bertaut's representation analysis method to *Pbcm* space group[19] is one of the eight one-dimensional irreducible representations with the magnetic arrangements shown in Table 4[20] where the Co1i and Co2i positions are the following: Co11 x, y, z; Co12 $-x, -y, -z$; Co13 $-x, -y, {}^1/_2 + z$; Co14 $x, y, {}^1/_2 - z$; Co15 $x, {}^1/_2 - y, -z$; Co16 $-x, {}^1/_2 + y, z$; Co17 $-x, {}^1/_2 + y, {}^1/_2 - z$; Co18 $x, {}^1/_2 - y, {}^1/_2 + z$; Co21 $x, y, {}^1/_4$; Co22 $-x, -y, {}^3/_4$; Co23 $-x, {}^1/_2 + y, {}^1/_4$; Co24 $x, {}^1/_2 - y, {}^3/_4$. The resulting observed and calculated profiles are given in Figure S8 (SI).

In this model (Figure 9), the magnetic moment of the Co(1) ion, M = 2.95(5) μ_B, is along the *c*-axis, the M_x and M_y components being not significant. For Co(2), the moment is aligned along the *c*-axis according to the irreducible representation but the magnetic moment, 3.31(6) μ_B, is significantly higher than the expected 3 μ_B spin-only value; this suggests some orbital contribution. In $CoSO_4$ for instance,[21] a value of 3.3(2) μ_B was observed at 4.2 K. However, compared to the manganese sample, the background appears completely flat at 1.4 K. In the former, the presence of a broad hump centered at a 2θ value around 30° was attributed to the concomitant existence of a short-range ordering (SRO). In short, the magnetic structure can be regarded as antiparallel orientation of the moments of two ferrimagnetic chains in the unit-cell, related by the center of inversion. Therefore the canting, which cannot be resolved from the neutron data, cannot originate from a Dzyaloshinskii mechanism[22] nor from Moriya's single-ion anisotropy mechanism.[23] For the present case, a hidden canting may be operative given that there are four asymmetric units within the magnetic unit cell.[24] Hidden canting occurs in systems consisting of four sublattices, where the resultant canted magnetization of a pair of sublattices is canceled by that of the other pair.

When the temperature is increased, the magnetic components of both Co(1) and Co(2) remain quite constant up to 25 K (Figure 10, Table S3). Above 25 K, they start to decrease and vanish between 37.5 and 40.5 K, i.e., a temperature slightly lower than the one observed by susceptibility measurements. One can also observe that the moment of Co(1) starts to decrease (25 K) before that of Co(2) (30 K).

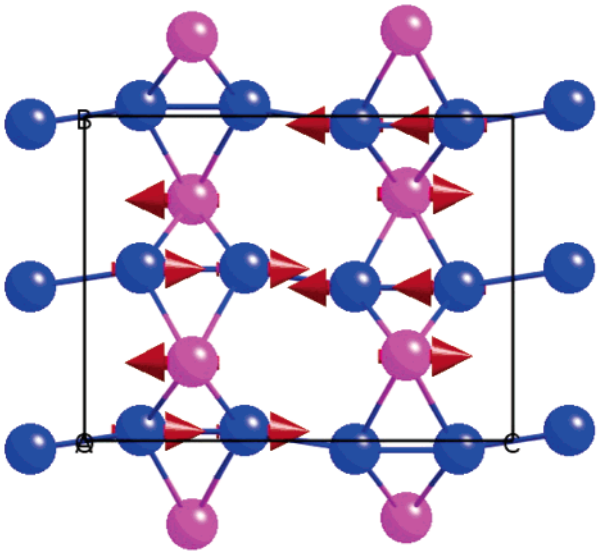

Figure 9. Orientation of the moments of Co1 (blue) and Co2 (purple) in the magnetic structure of $Co_3(OD)_2(SO_4)_2(D_2O)_2$.

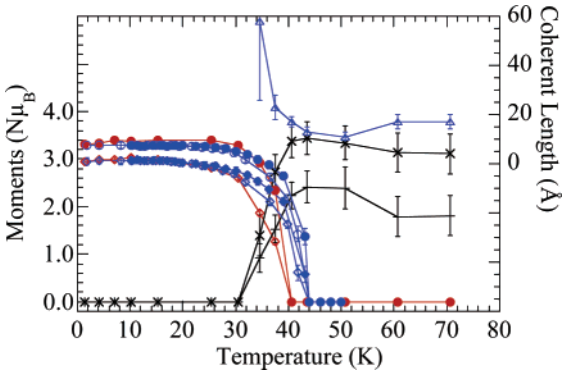

Figure 10. Temperature dependence of the *z*-component of the magnetic moments for the long-range-ordered part for Co1 (diamonds) and Co2 (circles) obtained from neutron refinements of the data from ILL (blue filled symbols for cooling and blue open symbols for warming up) and from Saclay (red symbols). Those for the short-range-ordered part for Co1 (plus) and Co2 (×) and the coherent length (blue triangles). Lines are guide to the eyes.

At 34 K, one observes a significant increase of the background that gives rise to a broad hump centered at around 30°. Such modification has been attributed to the appearance of a short-range (SRO) magnetic ordering. Assuming that the volume distribution of both phases, LRO and SRO, is homogeneous, we have refined the latter using the same model as for the former but with a different coherence length. One observes (Figure 10, Table S3) that the M_z components of both Co(1) and Co(2) ions increase up to 40.5 K where they reach a maximum around 50 K before decreasing at higher temperatures. The maximal values are then observed in the temperature region where the LRO structure disappears. The coherence length rapidly decreases from 58 Å at 34 K to around 15 Å above 40.5 K. Whereas the M_z component of Co(1) ion remains below 3 μ_B, the corresponding one for Co(2) ion reaches high values up to 3.4(3) μB at 40.5 and 43.6 K, values attributed to the difficulty to refine data from the broad hump. The SRO phase

(19) Bertaut, E. F. *Acta Crystallogr. A* **1968**, *24*, 217.
(20) (a) KAREP − a program for calculating irreducible space group representations. Hovestreydt, E.; Aroyo, I.; Sattler, S.; Wondratschek, H. *J. Appl. Crystallogr.* **1992**, 25, 544. (b) BASIREPS − a program for calculating nonnormalized basis functions of the irreducible representations of the little group Gk for atom properties in a crystal. Rodriguez-Carvajal, J.; Laboratoire Léon Brillouin (CEA-CNRS), CEA Saclay, Gif sur Yvette, France.
(21) Frazer, B. C.; Brown, P. J. *Phys. Rev.* **1962**, *125*, 1282−1291.
(22) Dzyaloshinskii, I. E. *Soviet Phys. JETP*, **1958**, *6*, 621.
(23) Moriya, T. *Phys. Rev.* **1960**, *117*, 635. Moriya, T. *Phys. Rev.* **1960**, *120*, 91.
(24) Silvera, I. F.; Thornley, J. H. M.; Tinkman, M. *Phys. Rev.* **1964**, *136*, 695.

is still observed at 70 K, the highest temperature of our measurements.

As pointed out in the magnetic measurements, a hysteresis was evidenced in the temperature dependence of the magnetization. To confirm this effect, neutron powder data have been collected on cooling and heating at a rate of 0.5 K/minute on the D20 ILL diffractometer. The reproducibility of the patterns compared to the ones recorded at LLB lead us to consider the same model for the LRO magnetic structure for the subsequent refinements, yielding close values for the cobalt magnetic moments. So, values of 2.95(5) and 2.97(6) μ_B for M_z (Co1), and 3.31(6) and 3.27(7) μ_B for M_z (Co2) are observed at 1.4 and 1.8 K from data at LLB and ILL, respectively. Otherwise, the hump is visible for the same temperature region. For the cooling and warming data collection at ILL (Figure 10), one observes that the calculated magnetic moments are not reversible between around 30 and 45 K, the region where the hysteresis was observed in the magnetic measurements. The structural model presented for the LRO magnetic phase does not reveal the canted moments suggested by the magnetic measurements. Indeed, the very small canting angle cannot be evidenced from powder neutron diffraction data. The magnetic model is antiparallel alignment of the moments. Some relations can be proposed between both results. No magnetic component is found along the *a*-axis, in agreement with the monotonic evolution of the susceptibility. For both crystals, the spontaneous magnetization is observed for applied field parallel to the *b*-axis. On the other hand, the magnetization tends to zero at low temperature for applied field along the *c*-axis, for which the M_z components are strictly antiparallel, resulting in a zero magnetization. For the *a*-axis, a slight anomaly was observed for crystal 1 and none for crystal 3 due to the better alignment of the latter. As the M_x magnetic components are always insignificant for Co(1) and strictly zero by symmetry for Co(2) ions, one expects a flat evolution of the susceptibility along this direction. The small drop at T_N for crystal 1 is, therefore, attributed to a misalignment compared to crystal 3. However, even for the latter, a small misalignment can induce a change at T_N. At this point of our discussion, it appears interesting to go back to the results obtained for the nickel and manganese compounds to look at the trends within the $M_3(OH)_2(SO_4)_2(H_2O)_2$ family according to the M cation.

Trends in the $M_3(OH)_2(SO_4)_2(H_2O)_2$ Family (M = Mn, Co, or Ni). Hydrothermal synthesis appears to be a good technique for the preparation of highly crystalline hydroxysulfates and single crystals large enough for SQUID magnetometry. Due to the relative instability of Mn^{2+} and Co^{2+} in aqueous solutions, some care has to be taken to prevent their oxidations. This is no more the case for nickel. In all cases, a mixture of two or more compounds is obtained. To promote the formation of single phases, several syntheses have been carried out with varying sodium hydroxide to metal sulfate molar ratios and the temperature of the reactions. However, we did not succeed to completely avoid the formation of the minor phases. However, one has to mention that the proportion of the secondary phase can be very low and is detected only by SQUID measurements; X-ray diffraction is unable to evidence their presence. Fortunately, in some cases the phases have different crystal shapes and/or colors and therefore, they can be separated under a microscope.

Table 5. Ionic Radii and Mean M−O Distances for $M_3(OH)_2(SO_4)_2(H_2O)_2$

M	ionic radius (Å)	⟨M(1)−O⟩ (Å)	⟨M(2)−O⟩ (Å)	⟨M−O⟩ (Å)
Mn	0.95	2.208	2.158	2.183
Co	0.8	2.117	2.083	2.100
Ni	0.74	2.087	2.049	2.068

The DT-TGA traces reveal a similar thermal evolution with three decomposition steps related to water loss, OH group departure, and sulfate decomposition. For Mn and Co, a last loss is related to the reduction of Mn_2O_3 or Co_3O_4 previously formed by oxidation of MnO or CoO. As revealed by the data in Table S4 (SI), the temperature of the maxima of the endothermal effects associated with the weight losses increases from Mn to Co and Ni for the water and OH groups ones. For SO_4 decomposition, an inversion is observed between Co and Ni that can be related to the existence of a high-temperature β-modification whose thermal stability is not the same as the one of the low temperature α-modification also adopted by $MnSO_4$ and $NiSO_4$.

The similarity evidenced for the thermal analysis is also observed in the case of the infrared spectra (Table S5, SI). Again a tendency for increased wavenumbers from Mn to Ni is observed. This evolution, reflecting the variation of force constant, is in agreement with the corresponding bond distances (Table 5) that decrease from Mn to Ni. The structure is strictly similar for the three compounds, with a slightly greater distortion of the MO_6 octahedra being observed for M = Mn. The M−O−M angle values that are related to the nature (AF or F) of the magnetic interactions do not significantly deviate from one compound to another.

Although the structures are basically the same, there exist certain differences. The first is the decrease of the volume of the unit-cell as a function of the ionic radius, Mn > Co > Ni. All the parameters such as M−O bond distances change accordingly. However, since the size of the sulfate remains unaltered, the corrugation of the sheets changes to accommodate the two different sulfate groups. As a result, the position of M2 in relation to the neighboring M1 in the plane is changed. This is seen as a very slight dissymmetry of the M2 in relation to M1 as exemplified by the M1−M2−M1 angles for the same M2 but for M1 of neighboring chains, being 51.11 and 51.15° for Mn, 51.39 and 50.72° for Co, and 50.33 and 51.22° for Ni. This large dissymmetry for nickel may be partly responsible for the different magnetic structures. We should also note that the equidistance of Mn2 to the four Mn1 atoms is a source of frustration of the triangular magnetic motif that may result in the large change in orientation of the magnetic moments for the manganese compound.

Concerning the magnetic properties recorded on powders, a similar temperature dependence of the magnetic susceptibility is evidenced with a sudden jump at T_N. The other behaviors, viz., a linear dependence of isothermal magnetization in the ordered state, no saturation limit, and sharp anomaly in the ac-susceptibilities, are characteristic of a

Table 6. Magnetic Data for $M_3(OH)_2(SO_4)_2(H_2O)_2$

M	T_N (K)	C (emu·K·mol M^{-1})	μ_{eff} (μ_B)	θ (K)	g	M_{5T} ($N\mu_B$)	H_c (Oe)	canting angle (deg)
Mn	26	4.92	6.27	−75	2.07	4.2	0	≅0
Co	42	3.06	4.95	−68	2.56	0.7	350	0.2
Ni	29	1.30	3.22	−31	2.29	0.7	1400	0.3

canted-antiferromagnet. However, the presence of a very minor impurity perturbs the interpretation of the results. Table 6 summarizes the magnetic data. The high g-value for the Co compound can be related to the influence of spin−orbit coupling. It can also be noticed that the Weiss θ value for the Ni compound is smaller than those for the other ones. Fortunately, single crystals big enough for magnetic measurements have been obtained with M = Co and allow a complete interpretation of the magnetic properties. These studies have been completed by the determination of the magnetic structures from neutron powder diffraction data.

Conclusion

This work confirms the structure of the titled compound and establishes the precise positions of the deuterium atoms from the neutron data and permitting high-resolution magnetic structure determination. Single-crystal magnetization measurements provide a textbook case for a clear definition of the easy (along *c*-axis), the hard (also the canting axis along *b*), and the intermediate (along *a*) axes of a canted-antiferromagnetic system that are in agreement with the magnetic structure determination. The observation of an unusual hysteresis in the temperature dependence of the magnetization and of the magnitude of the refined moments remains to be understood. Of interest of the physics of this compound is the existence of short-range and long-range magnetic orderings within a range of temperatures and this requires further studies.

Acknowledgment. This work was funded by the CNRS (France). We thank André Decian for collecting the single-crystal diffraction data and Jacques Faerber for indexing the crystals for magnetic measurements. M.B.S. thanks the "Ministère de l'Enseignement Supérieur de Tunisie" for a start-up thesis grant. We are grateful for the help of Drs. T. Hansen, M. A. Green, and A. Wills with the collection of the neutron data at ILL.

Supporting Information Available: Tables of X-ray single crystal and neutron powder diffraction data refinement at 300 K and at low temperatures; tables summarizing thermal effects and IR band frequencies for the Mn, Co and Ni equivalents; figures of DT-TGA traces, temperature-dependent X-ray diffraction patterns, IR spectra for hydrogenated and deuterated samples, observed and calculated powder neutron diffractions at 300 and 1.4 K (pdf). X-ray crystallographic data file (CIF). This material is available free of charge via the Internet at http://pubs.acs.org.

CM047790M